Pulse Expansion and Doppler Shift of Ultrahigh Intense Short Pulse Laser by Slightly Overdense Plasma

Hitoshi SAKAGAMI and Kunioki MIMA[1]

Department of Simulation Science, National Institute for Fusion Science, Toki 509-5292, Japan
[1]*Institute of Laser Engineering, Osaka University, Osaka 565-0871, Japan*

The interactions between ultrahigh intense laser and overdense plasmas were investigated by the use of a 1-1/2 dimensional electromagnetic relativistic particle-in-cell code, EMPAC. When the effective electron plasma frequency is reduced below the laser frequency by increasing the inertial electron mass due to the relativistic effect, the ultrahigh intense short pulse laser can penetrate the overdense plasma, but is completely reflected after propagating to a certain extent, except for a portion of the absorbed laser. The pulse length of the reflected laser is expanded more than that of the incident laser by a modulation due to the anomalous penetration, and the pulse expansion factor can be predicted by the schematic model. The frequency of the reflected laser can be calculated by the Doppler shift formula coupled with a relativistic dispersion relation, and is good agreement with the simulation result. The anomalously penetrating pulse shows soliton-like behaviors in the plasma after the incident laser has vanished.

1. Introduction

Recent developments in laser technology have made it possible to generate ultrahigh intense subpicosecond pulses, and experiments are now being carried out to explore new regimes of relativistic laser-plasma interactions [1–4]. When the plasma is irradiated by such intense lasers, electrons oscillating in the field of the laser wave are strongly relativistic. It was predicted that the ultrahigh intense laser would be able to propagate into a sufficiently overdense plasma by the relativistic electron mass correction and hence decrease the effective electron plasma frequency [5–7]. It was also reported that an *s*-polarized wave interacting with a sharp-boundary plasma has excited an electromagnetic nonlinear pulse with relativistic amplitude propagating into the overdense plasma [8], and the transition between an opacity and a transparency regime for the propagation of the ultrahigh intense laser into overdense plasmas has been discussed [9]. The recession velocity was found to be significantly reduced due to the relaxation-oscillation of the penetration that was coupled with the electron density oscillation at the laser front. The intensity threshold for the penetration was also found to depend on both plasma density and ion dynamics that were characterized by the ion acoustic speed [10]. Recently, the relativistic solitons in both underdense and overdense plasmas have been investigated theoretically and experimentally [11–16]. In this paper, we present the interactions between ultrahigh intense ($\geq 2 \times 10^{18}$ [W/cm²-µm²]) short

pulse (16 ~ 133 fs) lasers and slightly overdense (twice the critical density) plasmas by the use of a 1-1/2 dimensional electromagnetic relativistic particle-in-cell code, EMPAC [17].

Simulations were performed with immobile ions to inhibit plasma expansions into vacuum and to investigate relativistic electron dynamics; $T_e = 10$ keV, $\omega_{pe}\Delta t = 0.05$, $\lambda_{De}/\Delta = 1$, and the number of electrons per mesh = 200. The Gaussian laser pulse was launched from the right boundary, and the plasma was a thick slab with a constant density and sharp boundary edges. The simulation system is shown in Fig. 1. Long vacuum regions were appended on both sides of the plasma slab. Therefore, no artificial boundary condition, such as the reemission of escaping particles, was needed.
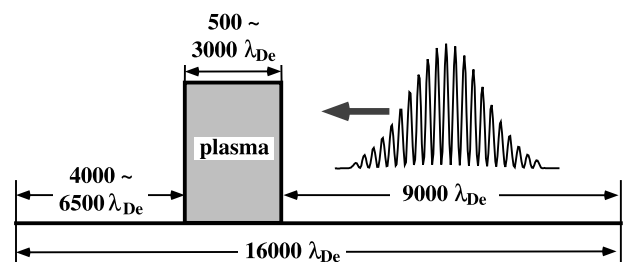

Fig. 1 The simulation system. Long vacuum regions are appended on both sides of the plasma slab.

author's e-mail: sakagami.hitoshi@nifs.ac.jp

2. Pulse Expansion

The ultrahigh intense short pulse laser can penetrate into the overdense plasma due to the relativistic effect, but is completely reflected after propagating to a certain extent except for a portion of the absorbed energy if the plasma is thick enough. As a typical result, the *x-t* diagram of the electromagnetic field intensity and the incident and reflected pulse shapes are shown in Fig. 2 for $I_L\lambda_L^2 = 2 \times 10^{19}$ [W/cm^2-μm^2] and FWHM (Full Width at Half Maximum) = $5\lambda_L$, where I_L is the peak laser intensity and λ_L is the laser wavelength in microns. The leading edge of the pulse is immediately reflected by the plasma because the temporal intensity is not enough to accelerate electrons up to the relativistic velocity and to trigger the anomalous penetration. The main part of the pulse, however, can penetrate into the plasma and propagate until the reflection at the recession front, where a discontinuity between the perturbed and unperturbed plasma exists, acting as a moving mirror. Thus, the shape of the pulse is changed and the pulse length of the reflected laser is expanded more than that of the incident laser by a modulation due to the anomalous penetration.

The higher the intensity, the deeper the pulse penetrates into the plasma from the boundary, but the laser is finally reflected back when no energy is supplied at the recession front to sustain the permeation. The simulation results of the pulse expansion factor, which is defined as a ratio of the incident and reflected laser pulse lengths, are shown in Fig. 3 for various laser intensities and pulse durations. Deeper anomalous penetration causes a longer traveling time and leads to more pulse modulation and expansion. It should also be noted that the laser pulse durations have a minimal effect on the expansion factors.

The frequency of the reflected laser can be calculated by the matching condition of the Doppler shift formula coupling with the relativistic dispersion relations [18] as follows:

$$\frac{\omega_r}{\omega_L} = \frac{u_f/c - v_{prop}/c}{u_f/c} \cdot \frac{u_b/c}{u_b/c + v_{prop}/c} \qquad (1)$$

$$\frac{u_f}{c} = 1 \bigg/ \sqrt{1 - \frac{n_0}{n_{cr}\gamma}} \qquad (2)$$

$$\frac{u_b}{c} = 1 \bigg/ \sqrt{1 - \frac{n_0}{n_{cr}\gamma \left(\omega_r/\omega_L\right)^2}} \qquad (3)$$

where v_{prop} is the propagation velocity of the recession front, c is the light speed in vacuum, n_0 is the plasma density, n_{cr} is the critical density, and γ is the Lorentz factor, and u_f, u_b, ω_L and ω_r are the phase velocities of the forward and backward laser in the plasma, the frequencies of the incident and reflected laser, respectively. Ignoring the oscillation in the longitudinal field, the simple estimation for γ is obtained as follows [19]:

$$\gamma = \sqrt{1 + \frac{I_L\lambda_L^2}{1.37 \times 10^{18}}}. \qquad (4)$$

As v_{prop} is evaluated by the trajectory of the recession front in the *x-t* diagram of the electromagnetic field intensity for different laser intensities but a fixed pulse length (FWHM = $10\lambda_L$), the predicted frequencies of the reflected lasers can be calculated with Eqs. (1)-(4) and are shown in Fig. 4 as circles. The time averaged spectral intensity of the reflected laser can also be observed in the simulations, and the frequency of the maximum amplitude in the spectrum is shown in Fig. 4 as crosses. Analytical values were found to be good agreement with the simulation results, and we can conclude that the frequency downshift in the reflected laser is caused by the Doppler shift at the recession front.
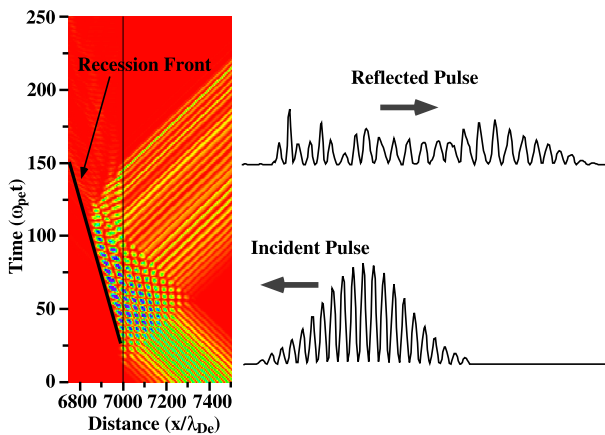

Fig. 2 The *x-t* diagram of the electromagnetic field intensity, and the incident and reflected pulse shapes for $I_L\lambda_L^2 = 2 \times 10^{19}$ [W/cm^2-μm^2], FWHM = $5\lambda_L$. The plasma exists at $4000 \leq x/\lambda_{De} \leq 7000$.
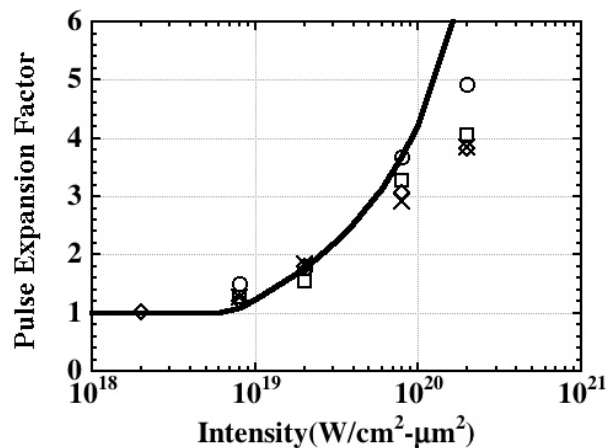

Fig. 3 The pulse expansion factor as a function of the laser intensity obtained by simulations. Circle, square, diamond and cross indicate FWHM = $2.5\lambda_L$, 5, 10 and 20, respectively. The solid line indicates the pulse expansion factor predicted by the schematic model.
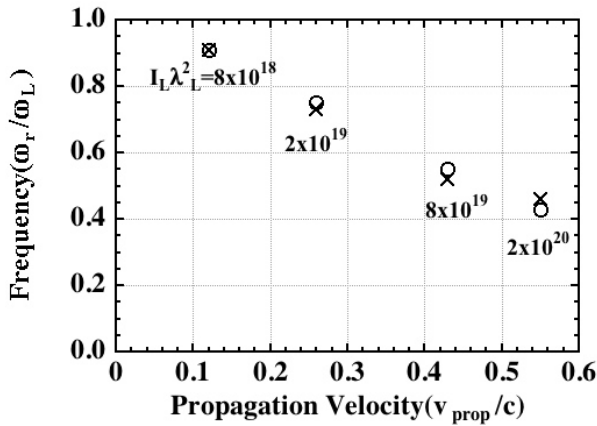
Fig. 4 The frequency of the reflected laser as a function of the propagation velocity which depends on the laser intensity. The pulse length of the incident laser is fixed to FWHM = $10\lambda_L$. Circle and cross indicate the predicted value and the simulation result, respectively.

Fig. 5 The schematic model for the pulse expansion.

We assumed that the incident laser pulse can be divided into three portions, a leading portion in which the laser intensity is below that of the threshold for the anomalous penetration (we defined the pulse length of this portion as L_{ref}), the main portion with an over threshold intensity (L_{in}), and a trailing portion with a below threshold intensity (L_{ref}). The leading portion is immediately reflected at the plasma boundary, and also becomes the leading portion of the reflected laser pulse. The main portion penetrates into the plasma and propagates with the group velocity v_{g2}, and is reflected at the recession front, which propagates with v_{prop}. After reflection, it propagates with the different group velocity v_{g3} because the frequency is changed due to the Doppler shift. The trailing portion is also reflected at the plasma boundary, and is superimposed on the reflected main laser pulse. This schematic model for the pulse expansion is shown in Fig. 5.

According to this schematic model, the pulse length of the reflected main portion can be calculated as follows:

$$\frac{L_{out}}{L_{in}} = \frac{v_{prop}}{v_{g2} - v_{prop}} \cdot \frac{v_{g3} + v_{g2}}{v_{g3}} + 1 \qquad (5)$$

where v_{g2} and v_{g3} are defined [18] as follows:

$$\frac{v_{g2}}{c} = \sqrt{1 - \frac{n_0}{n_{cr}\gamma}} \qquad (6)$$

$$\frac{v_{g3}}{c} = \sqrt{1 - \frac{n_0}{n_{cr}\gamma (\omega_r/\omega_L)^2}}. \qquad (7)$$

Finally the pulse expansion factor can be derived as follows:

$$F_{exp} = \frac{L_{out} + L_{ref}}{L_{in} + 2L_{ref}}. \qquad (8)$$

The Gaussian pulse is cut at 1 % of the peak intensity in simulations, and this gives the pulse length $L_{in} + 2L_{ref}$.
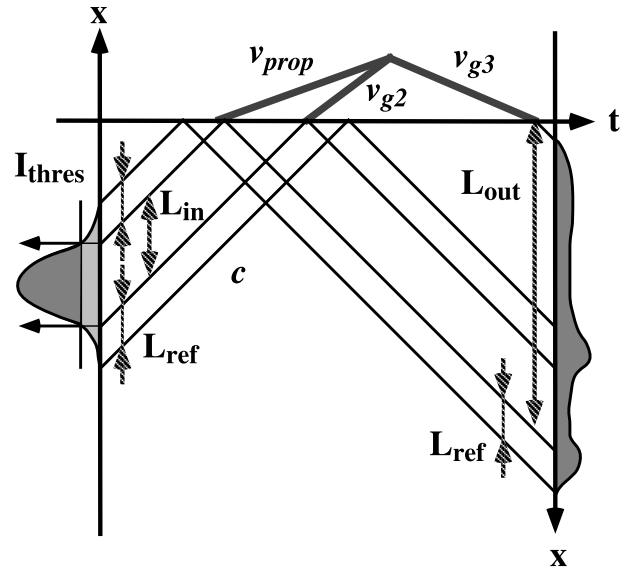
As the plasma density is twice the critical density, the threshold intensity can be calculated to $I_{thres} = 4.11 \times 10^{18}$ from Eq. (4) with $\gamma = 2$, and this gives L_{in}. The pulse expansion factor of the schematic model is shown in Fig. 3 as a solid line, and is in good agreement with the simulation results in the case of $I_L\lambda_L^2 \leq 10^{20}$ [W/cm²-µm²]. When the laser intensity is higher than 10^{20} [W/cm²-µm²], the main portion adjacent to the trailing portion must propagate deeper inside the plasma before the reflection at the recession front, and travel a longer path to the boundary even after the reflection. As the incident pulse loses its energy due to absorption by the plasma, it cannot reach the boundary, and will not launch the electromagnetic energy to vacuum. Thus the pulse length of the reflected laser should be shorter than that by the schematic model. Note that the reflected laser pulse actually propagates in not as simple a manner as that described above. We will discuss this feature in the next section.

3. Solitary Structure

The anomalously penetrating pulse shows soliton-like behaviors in the plasma after the incident laser has vanished. The x-t diagram of the electromagnetic field intensity is shown in Fig. 6 for $I_L\lambda_L^2 = 8 \times 10^{19}$ [W/cm²-µm²] and FWHM = $10\lambda_L$. As one wavepacket collides with another and then overtakes it, the individual reflected wavepackets seem to propagate independently like a soliton.

The wavepacket can accelerate electrons and the local effective Lorentz factor increases; hence this leads to an increase of the local refraction index. The wavepacket is trapped by the plasma which has a larger refraction index, more than that of its surroundings, and accelerates electrons much more. These processes construct positive feed-
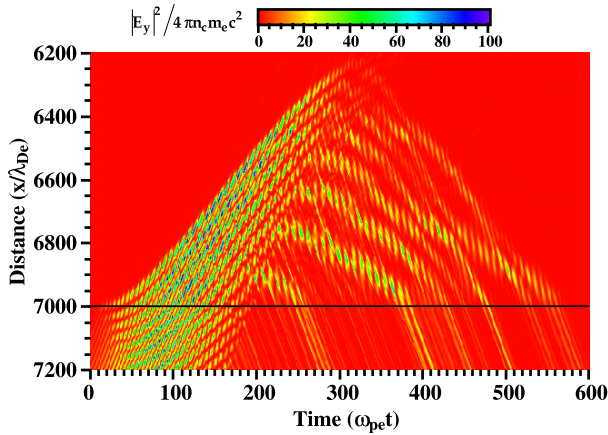
Fig. 6 The *x-t* diagram of the electromagnetic field intensity for $I_L \lambda_L^2 = 8 \times 10^{19} [\text{W/cm}^2\text{-}\mu\text{m}^2]$, FWHM $= 10\lambda_L$. The plasma exists at $4000 \leq x/\lambda_{De} \leq 7000$.

Fig. 8 The *x-t* diagram of the electromagnetic field intensity for the same parameters as in Fig. 6 except the thin plasma. The plasma exists only at $6500 \leq x/\lambda_{De} \leq 7000$.
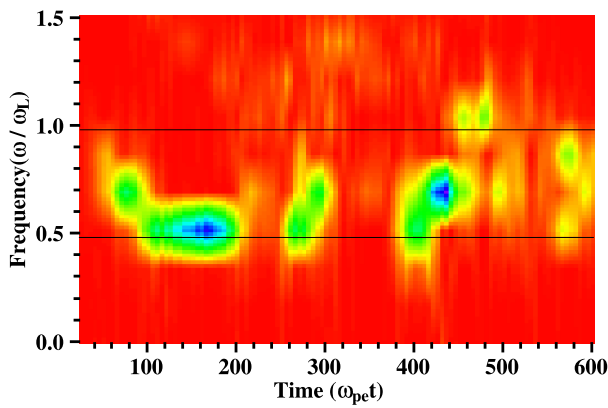

Fig. 7 The time evolution of the spectral intensity of the reflected pulse for the same parameters as in Fig. 6. The spectral intensity is observed at $x/\lambda_{De} = 7200$.

Fig. 9 The time evolution of the spectral intensity of the transparent (a) and reflected pulses (b) for the same parameters as in Fig. 8. The spectral intensities are observed at $x/\lambda_{De} = 6300$ for the transparent laser and at $x/\lambda_{De} = 7200$ for the reflected laser

back and compensate for energy absorption by the plasma, keeping the wavepacket as stable as a solitary structure. It was observed in the simulation results that the local effective plasma frequency along the trajectory of the solitary structures was smaller than the value of the surroundings. It was noted that the average electron density was unchanged from the initial value due to immobile ions and that it does not affect the refraction index.

The time evolution of the spectral intensity of the reflected pulse is shown in Fig. 7 for the same parameters as in Fig. 6. The peak intensity of $\omega/\omega_L \sim 0.5$ around $\omega_{pe}t \sim 160$ corresponds to the laser reflected at the recession front described in the previous section. The reflected pulse also exhibits the soliton-like propagation, which causes delayed emissions [13] after $\omega_{pe}t \sim 260$ with different frequencies from that of the major reflected laser.

The *x-t* diagram of the electromagnetic field intensity for a thin plasma is shown in Fig. 8 and the corresponding time evolution of the spectral intensity of the transparent
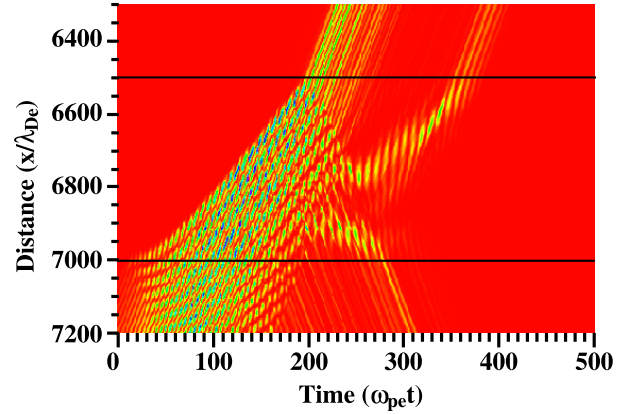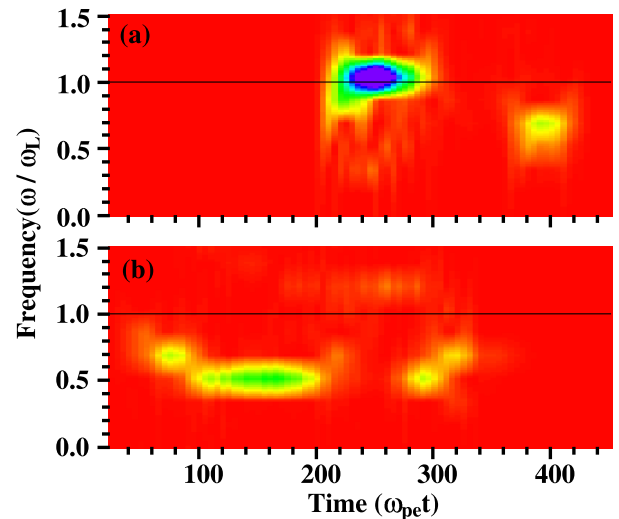
and reflected pulses are shown in Fig. 9 with the same parameters as in Fig. 6. The peak intensity of the transparent pulse around $\omega/\omega_L \sim 1$ and $\omega_{pe}t \sim 240$ in Fig. 9 (a) coincides with the anomalously penetrating pulse, which is not reflected inside the plasma. The intensity around $\omega/\omega_L \sim 0.5$ and $100 \leq \omega_{pe}t \leq 190$ in Fig. 9 (b) coincides with the laser reflected at the recession front. The delayed emission around $\omega_{pe}t \sim 300$ in Fig. 9 (b) is also caused by the reflected solitary structure. When the plasma is sufficiently thick, hot electrons generated by the ultrahigh intense pulse run away from the interaction region and the inner state of the plasma remains unchanged. If the plasma is thin, however, it is filled up with the hot electrons and the properties of the plasma may vary. In this case, one
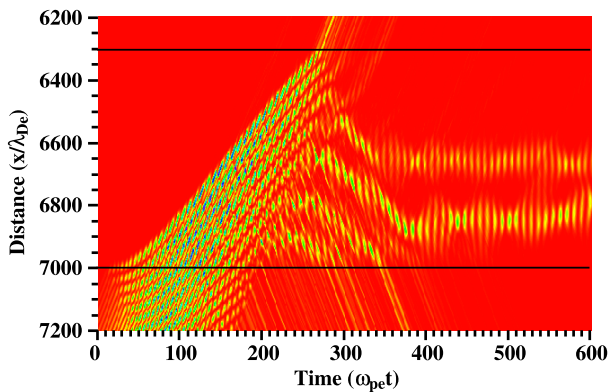
Fig. 10 The *x-t* diagram of the electromagnetic field intensity for the same parameters as in Fig. 6, except the plasma width. The plasma exists at $6300 \leq x/\lambda_{\mathrm{De}} \leq 7000$, which is thinner than that in Fig. 6 but thicker than that in Fig. 8.

solitary structure turns and propagates in the opposite direction throughout the whole plasma, and also causes delayed emission at the other boundary around $\omega_{\mathrm{pe}}t \sim 400$ in Fig. 9 (a). As this transparent soliton was originated from the reflected pulse, the frequency is the same as that of the reflected pulse, $\omega/\omega_{\mathrm{L}} \sim 0.5$.

The *x-t* diagram of the electromagnetic field intensity for a medium width plasma is shown in Fig. 10. In this case, a part of the incident laser passes through the plasma, another part is reflected at the recession front and launched into a vacuum the same as in the previous case, but two reflected solitons come to rest inside the plasma. Thus it was found that the propagation direction of the soliton would be affected by the plasma width.

4. Summary

We have investigated, through a series of simulations with the 1-1/2 dimensional electromagnetic relativistic particle-in-cell code EMPAC, the anomalous penetration. An ultrahigh intense short pulse laser could penetrate into the overdense plasma by increasing the inertial electron mass and hence decreasing the effective electron plasma frequency, but it was found to be completely reflected after propagating to a certain extent. The pulse length of the reflected laser was expanded more than the incident pulse length by a modulation due to the anomalous penetration, and the pulse expansion factor could be predicted by the schematic model. The frequency of the

reflected laser could be calculated by the Doppler shift formula coupled with a relativistic dispersion relation, and was in good agreement with the simulation results. The anomalously penetrating pulse showed soliton-like behaviors in the plasma after the incident pulse had vanished. When the plasma is thin, the solitary structure turns and propagates through the plasma, and launches the low frequency pulse at the opposite edge. If the plasma is medium width, the soliton becomes stationary inside the plasma. Unfortunately, the characteristics of the solitary structure, such as the relation between an amplitude and a propagation speed and the propagation direction, are not obvious, and more discussion and research is needed.

[1] P. Main, and G. Mourou, Opt. Lett. **13**, 467 (1988).
[2] M.D. Perry, F.G. Patterson and J. Weston, Opt. Lett. **15**, 381 (1990).
[3] F.G. Patterson, R. Gonzales and M.D. Perry, Opt. Lett. **16**, 1107 (1991).
[4] G.A. Mourou, C.P.J. Barty and M.D. Perry, Phys. Today **511**, 22 (1998).
[5] A.I. Akhiezer and P.V. Polovin, Sov. Phys. JETP **3**, 696 (1956).
[6] P. Kaw and J. Dawson, Phys. Fluids **13**, 472 (1970).
[7] A.D. Steiger and C.H. Woods, Phys. Rev. A **5**, 1467 (1972).
[8] S.V. Bulanov, N.M. Naumova and F. Pegoraro, Phys. Plasmas **1**, 745 (1994).
[9] E. Lefebvre and G. Bonnaud, Phys. Rev. Lett. **74**, 2002 (1995).
[10] H. Sakagami and K. Mima, Phys. Rev. E **54**, 1870 (1996).
[11] T.Zh. Esirkepov, F.F. Kamenets, S.V. Bulanov and N.M. Naumova, JETP Lett. **68**, 36 (1998).
[12] S.V. Bulanov, T.Zh. Esirkepov, N.M. Naumova, F. Pegoraro and V.A. Vshivkov, Phys. Rev. Lett. **82**, 3440 (1999).
[13] S.V. Bulanov, T.Zh. Esirkepov, F. Califano, K. Mima, N.M. Naumova, K. Nishihara, F. Pegoraro, Y. Sentoku and V.A. Vshivkov, J. Plasma Fusion Res. **75**, 75 (1999).
[14] Y. Sentoku, T.Zh. Esirkepov, K. Mima, K. Nishihara, F. Califano, F. Pegoraro, H. Sakagami, Y. Kitagawa, N.M. Naumova and S.V. Bulanov, Phys. Rev. Lett. **83**, 3434 (1999).
[15] N.M. Naumova, S.V. Bulanov, T.Zh. Esirkepov, D. Farina, K. Nishihara, F. Pegoraro, H. Ruhl and A.S. Sakharov, Phys. Rev. Lett. **87**, 185004 (2001).
[16] M. Lontano, S.V. Bulanov, J. Koga, M. Passoni and T. Tajima, Phys. Plasmas **9**, 2562 (2002).
[17] C.K. Birdsall and A.B. Langdon, *Plasma Physics via Computer Simulation* (McGraw-Hill, New York, 1982) p.181.
[18] S. Guerin, P. Mora, J.C. Adam, A. Heron and G. Laval, Phys. Plasmas **3**, 2693 (1996).
[19] S.C. Wilks, W.L. Kruer, M. Tabak and A.B. Langdon, Phys. Rev. Lett. **69**, 1383 (1992).